Design principles for the optimization of guest binding in aromatic-paneled $Fe^{II}_4L_6$ cages

Tanya K. Ronson, Wenjing Meng and Jonathan R. Nitschke*

Department of Chemistry, University of Cambridge, Lensfield Road, Cambridge, CB2 1EW, UK.

ABSTRACT: A series of aromatic-paneled $Fe^{II}_4L_6$ cages was synthesized through iron(II)-templated subcomponent self-assembly of 2-formylpyridine and C_2-symmetric diamine building blocks having differing geometries, including many with a large degree of lateral offset between metal-binding sites. The new cages were characterized using X-ray crystallography, NMR and mass spectrometry. Investigations of the guest binding properties of the cages provided insights into the structural factors important for the observation of guest binding. Both the size and arrangement of the aromatic panels were shown to be crucial for achieving effective encapsulation of large hydrophobic guests, including fullerenes, polycyclic aromatic hydrocarbons, and steroids, with subtle differences in the structure of subcomponents resulting in incommensurate effects on the binding abilities of the resulting hosts. Cages with large, offset aromatic panels were observed to be the most effective hosts as a result of a preference for a ligand conformation where the aromatic panels lie tangent to the edges of the tetrahedron, thus maximizing cavity enclosure.

Introduction

The study of self-assembled metal-organic cages[1] within the wider context of container molecules[2] has been a topic of great interest in recent years. The selective guest encapsulation properties of these structures[3] have led to their application in trapping and stabilization of unstable species,[4] separation of substrates as diverse as gases[5] and fullerenes,[6] the discrimination of chiral guest species[7] and as catalysts,[8] sensors[9] and photoreactors.[10] In order to extend the range of applications of this class of synthetic receptors, it is necessary to create hosts capable of tightly and selectively binding large substrates. The selective encapsulation of large aromatic molecules[11] such as fullerenes[6] and polycyclic aromatic hydrocarbons (PAHs)[12] is an attractive goal since the physicochemical properties of members of these classes of molecules are similar, which can render their separation difficult. Furthermore, PAHs are toxic and carcinogenic pollutants, rendering their selective encapsulation of interest for environmental decontamination.[13]

In order to design metal-organic cages with functional cavities,[14] several criteria must be met. Most importantly, the surface of the cage must be sufficiently enclosed to entrap guests inside[15] while being flexible enough to allow guests to enter and exit the host. The cavity must also provide a good size and shape match for targeted guests. Strong host-guest interactions can be further facilitated by cage walls with extended aromatic surfaces to provide favorable stacking interactions with aromatic guests.[16] One approach to achieving these criteria is to employ ligands with extended aromatic panels, which act both to enclose the cavity and undergo aromatic stacking interactions with prospective guests.[2d,17]

Others and our group have reported the formation of a variety of M_4L_6 metal-organic tetrahedra[18] of different shapes and sizes with diverse molecular recognition properties using subcomponent self-assembly.[19] This approach relies upon metal template effects to generate complex structures from simple molecular precursors through the formation of both dynamic-covalent (C=N) and coordinative (N→Metal) linkages in a single reaction step.[20] The properties of the resulting assemblies may be readily altered through variation or substitution of the subcomponents employed.[21] Small differences in the structure of a subcomponent can often produce major changes in the recognition properties of the assembly.[22]

Herein we explore this principle through an investigation of the parameters governing guest binding in a series of nine $Fe^{II}_4L_6$ tetrahedral cages prepared from iron(II), 2-formylpyridine and C_2-symmetric diamines with aromatic spacers of different geometries. The new cages were structurally characterized by single-crystal X-ray diffraction, and their guest-binding abilities were investigated in solution, revealing novel low-temperature behavior in several cases.

The combination of crystal structure information with solution-state binding data allowed for new structure-property relationships to be deduced. Offset aromatic spacers were observed to optimize the generation of enclosed cavities suitable for the encapsulation of large hydrophobic guests, whereas cages based on more linear ligands had more porous cavities and lower guest-binding affinities. The size of the aromatic panels was also crucial for determining the optimum size of guest for each cage, with differing selectivity towards the PAHs observed across the series of cages, as detailed below.

Results and Discussion

Self-assembly and X-ray crystal structures of aromatic-panelled $M^{II}_4L_6$ cages. Diamine subcomponents **A** – **G** were each synthesized in a single step from commercially available starting materials *via* Pd-catalyzed Suzuki-Miyaura cross-coupling[23] of 4-aminophenylboronic acid pinacol ester with an appropriate dibrominated derivative. Full descriptions of their syntheses are provided in the Supporting Information.

Scheme 1. Subcomponent self-assembly of $M^{II}_4L_6$ tetrahedral cages 1-9[a] from diamines A-F.

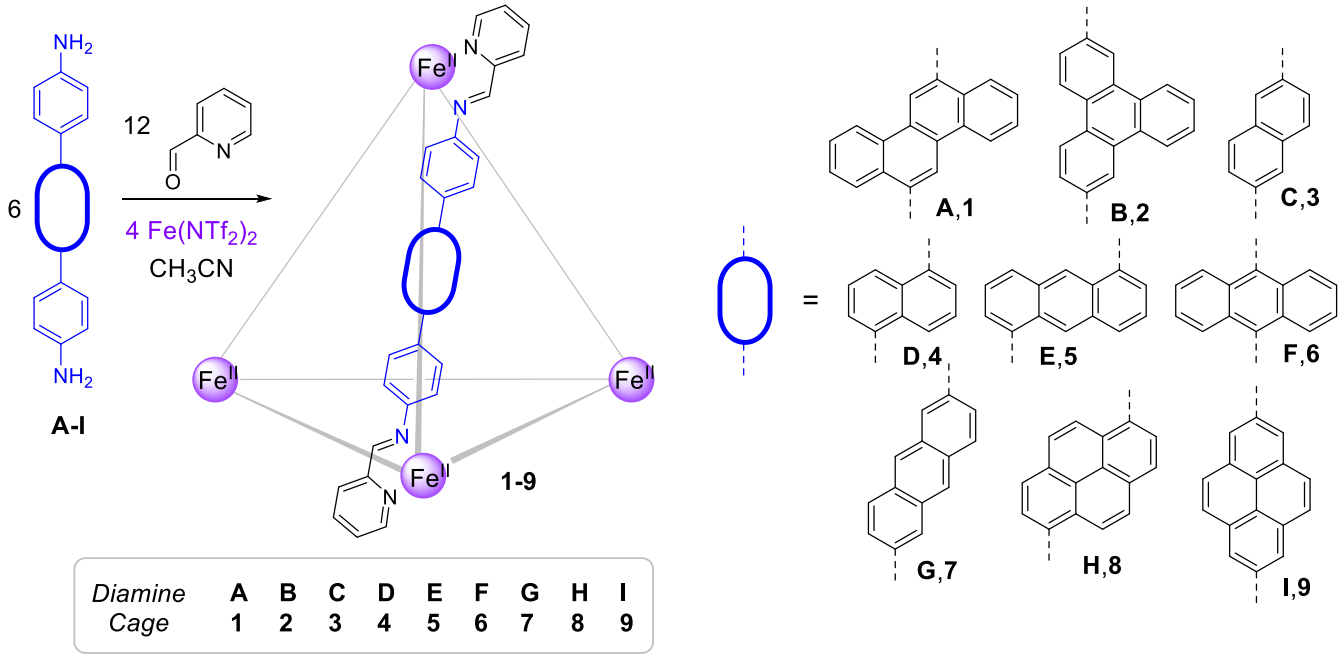

[a]Cages **5**, **8** and **9** were reported previously.[22,24]

The reactions of diamines **A** – **I** (6 equiv) with 2-formylpyridine (12 equiv) and iron(II) bis(trifluoromethane)sulfonimide ($Fe(NTf_2)_2$, 4 equiv) in acetonitrile at 323 K for 24 hours yielded tetrahedral cages **1** – **9** (Scheme 1). Cages **5**, **8** and **9** were reported previously, with full crystallographic characterization having been carried out on **5** and **9**.[22,24] ESI-MS confirmed the $Fe^{II}_4L_6$ composition of the assemblies, where L is the *bis*(pyridylimine) ligand derived from imine condensation of the respective diamine with 2-formylpyridine. The ^1H and ^{13}C NMR spectra of the new cages contained clusters of peaks, consistent with a mixture of homochiral *T* (ΔΔΔΔ/ΛΛΛΛ),[25] heterochiral C_3 (ΔΔΔΛ/ΛΛΛΔ), and achiral S_4 (ΔΔΛΛ)[26] diastereomers[27] in equilibrium, as has been observed for other cages prepared *via* subcomponent self-assembly.[22,28] Deconvolution of the imine region of the ^1H NMR spectra allowed the ratio of the diastereomers to be quantified[28a] in all cases except for **1** and **2** where quantification was precluded by insufficient dispersion of signals and signal overlap. In all cases DOSY NMR confirmed that the aromatic signals corresponded to species of similar size.

The solid-state structures of **1**, **2**, **3**, **4**, **6** and **7** were determined by single-crystal X-ray analysis. X-ray quality crystals of 6,12-chrysene-edged cage **1** were obtained from vapor diffusion of diisopropyl ether into an acetonitrile solution of **1**·8NTf_2 containing excess $KAsF_6$. Cage **1** crystallized in tetragonal space group I 41/a, with one quarter of a cage molecule in the asymmetric unit. The crystals were found to contain the achiral S_4 (ΛΛΔΔ) diastereomer (Figure 1). Of the six ligands that bridge the four octahedral iron(II) centers, four thus displayed a *syn*-conformation, bridging iron(II) centers of opposing handedness, and two adopted an *anti*-conformation, linking iron(II) centers of identical handedness. The metal-metal separations are in the range 18.4-18.5 Å. The four *syn*-ligands adopt a conformation in which the chrysene moieties lie almost tangentially to the edges of the tetrahedron, an arrangement expected to maximize the degree of cavity enclosure and favor efficient guest encapsulation. The *anti*-ligands are disordered around a C_2 axis but on average partially occupy the cavity of the tetrahedron. Consequently some faces of the tetrahedron are almost completely enclosed while other faces have pores of ca. 3.4 Å in diameter (see Figure S143).

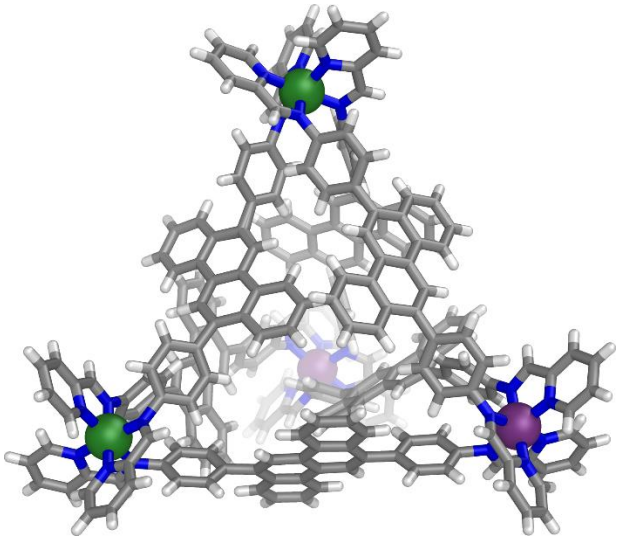

Figure 1. Cationic part of the crystal structure of **1**-S_4. Counterions, solvents and disorder are omitted for clarity. Δ and Λ Fe^{II} centers are colored purple and green, respectively.

X-ray quality crystals of 2,7-triphenylene-edged cage **2** were obtained from vapor diffusion of benzene into an acetonitrile solution of **2**·8NTf_2 containing excess Me_4NBF_4. Cage **2** crystallized in the monoclinic space group P 2/n with one complete cage in the asymmetric unit. Unusually, two cage diastereomers, **2**-C_3 and **2**-S_4, were observed to co-crystallize on the same lattice position, with an entire

tris(pyridylimine) iron(II) vertex disordered over two orientations of opposite handedness. One disordered part (with refined occupancy of 0.57) corresponds to the C_3-symmetric diastereomer (ΔΔΔΛ/ΔΛΛΛ) while the other part (of occupancy 0.43) with the opposite handedness corresponds to the S_4-symmetric diastereomer (ΔΔΛΛ). The structures of **2**-C_3 and **2**-S_4 are shown in Figure 2 and Figure S144 respectively. The iron(II) vertices are separated by distances of 20.7-21.1 Å (average 20.9 Å). The majority of the triphenylene panels adopt an approximately coplanar arrangement with the faces of the tetrahedron, resulting in large face pores of up to 10 Å in diameter (see Figure S146). In addition, the triphenylene edges are largely directed towards the exterior of the cage, further enhancing pore area.

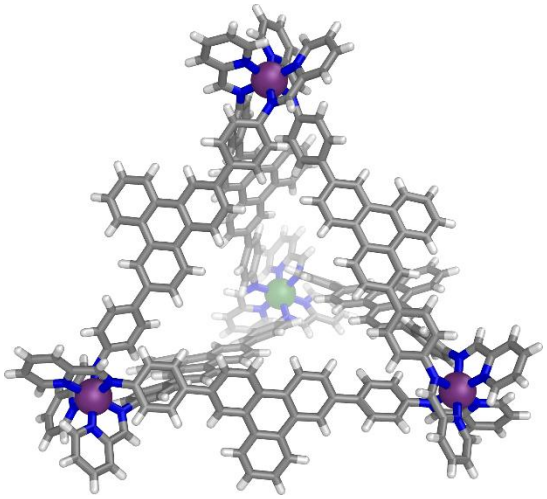

Figure 2. View down the pseudo-C_3-axis of the cationic part of the crystal structure of **2**, showing the ΔΔΔΛ enantiomer of the C_3-diastereomer. Counterions, solvents and disorder are omitted for clarity. Δ and Λ Fe^{II} centers are colored purple and green, respectively.

X-ray quality crystals of 2,6-naphthalene-edged cage **3** were obtained from vapor diffusion of benzene into an acetonitrile solution of **3**·8NTf_2 containing excess $KAsF_6$. Cage **3** crystallized in monoclinic space group C 2/c with half of a cage molecule in the asymmetric unit. As observed in the case of **1**, the crystals were found to contain the achiral S_4 (ΛΛΔΔ) diastereomer. The iron(II) centres are separated by distances of 18.8 – 19.4 Å (average 19.1 Å) which are slightly longer than in cage **1** despite their predicted similarity due to a slight bending of the ligands in the former case. The smaller aromatic panels of **3** relative to **1** render the surface much less enclosed with pores of up to 5.2 Å in diameter (see Figure S148). In solution **3** was found to exist as a mixture of 13% **3**-*T*, 49% **3**-C_3 and 38% **3**-S_4 respectively, almost identical to the expected statistical distribution of 12.5% *T*, 50% C_3 and 37.5% S_4, suggesting that the three diastereomers are of similar energy.

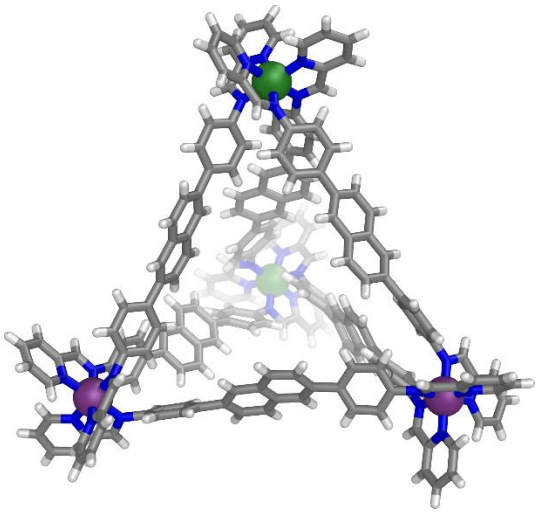

Figure 3. Cationic part of the crystal structure of **3**-S_4. Counterions, solvents and disorder are omitted for clarity. Δ and Λ Fe^{II} centers are colored purple and green respectively.

X-ray quality crystals of 1,5-naphthalene-edged cage **4** were obtained from vapor diffusion of diisopropyl ether into an acetonitrile solution of **4**·8NTf_2 containing excess Bu_4NReO_4. Cage **4** crystallized in trigonal space group $R\bar{3}c$, with one third of a cage molecule in the asymmetric unit. The C_3-symmetric diastereomer was found to have crystallized (Figure 4), with both ΛΛΛΔ and ΔΔΔΛ enantiomers present in the unit cell, related by inversion symmetry. Of the six ligands, three ligands display a *syn* conformation, bridging iron(II) centers of opposing handedness, and three adopt an *anti* conformation, linking iron(II) centers of the same handedness. The iron(II) vertices are separated by distances of 16.8 - 17.0 Å (average 16.9 Å).

The naphthalene units lie tangentially to the edges of **4**, affording an enclosed cavity with pores of ca. 2 Å in diameter (see Figure S150). Although the Fe-Fe distances in **4** are only slightly shorter than in the previously-reported 1,5-anthracene-edged analog **5** (average Fe-Fe 17.1 Å),[24] the cavity of **5** was significantly more enclosed, with pores of less than 1.4 Å in diameter.[24] In solution, **4** was found to exist as a mixture of 6% **4**-*T*, 46% **4**-C_3 and 48% **4**-S_4, respectively. The *T* isomer of **4** is thus slightly disfavored with respect to the statistical distribution, while the S_4 and C_3 diastereomers are slightly favored. We infer that the naphthalene units favor the *syn* ligand conformation found in the S_4 and C_3 diastereomers, which contain four and three *syn*-bridging ligands, respectively, over the *anti*-conformation required to bridge metal centers of the same handedness in the *T*-diastereomer. In contrast cage **5** exists solely as the *T*-diastereomer in solution and the solid state.[24] The greater degree of offset between binding sites in anthracene-edged **5** than in naphthalene-edged **4** may result in greater strain for the mixture of *syn* and *anti* ligands incorporated into the S_4 and C_3 frameworks in **5**, disfavoring these isomers with respect to *T*, as has been observed in other cases.[29]

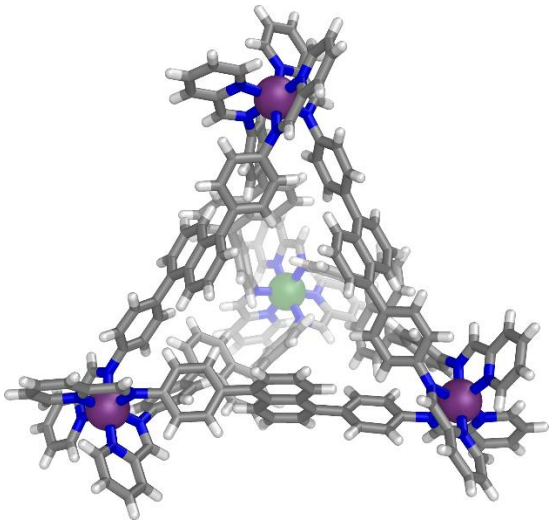

Figure 4. View down the C_3-axis of the cationic part of the crystal structure of **4**-C_3 showing the ΔΔΔΔ enantiomer. Counterions, solvents and disorder are omitted for clarity. Δ and Λ Fe^{II} centers are colored purple and green, respectively.

X-ray quality crystals of 9,10-anthracene-edged cage **6** were obtained from vapor diffusion of diisopropyl ether into an acetonitrile solution of **6**·8NTf_2 containing excess Bu_4NPF_6. Cage **6** crystallized in the monoclinic space group *P*21/n with two complete cage molecules in the asymmetric unit. The S_4-symmetric diastereomer was found to have crystallized (Figure 5). In solution cage **6** was found to exist as a mixture of 4% **6**-*T*, 55% **6**-C_3 and 41% **6**-S_4. As with cage **4**, the *T* isomer was thus disfavored with respect to the statistical distribution, while the S_4 and C_3 diastereomers are favored, indicating a preference for the *syn* ligand conformation. We infer that the steric bulk of the anthracene moiety obliges the two terminal phenylene rings to lie orthogonal to the anthracene, and thus coplanar with each other, in the lowest-energy conformation as observed in the solid-state structure of **6**. This preference for the *syn* ligand conformation agrees with previous observations in the case of a bulky (tetramethyl)terphenylene-based ligand.[28a]

The metal-metal separations in **6** are in the range 16.9–17.2 Å (average 17.1 Å), similar to those observed for the 1,5-anthracene isomer **5** but significantly shorter than in the 2,6-anthracene isomer **7**. The anthracene panels adopt conformations ranging from tangential to the cage edges to parallel with the cage faces. Consequently, the surface is less enclosed than the similarly sized **5**, where all anthracene panels adopt a conformation tangential to the edges of the tetrahedron.[24] The anthracene signals in the ^{1}H NMR spectrum of **6** are significantly broadened at 298 K, consistent with an intermediate rate of rotation on the NMR timescale, potentially as a result of gearing between anthracene panels on adjacent edges. Cooling the solution to 238 K led to a sharpening and increase in the number of anthracene signals in the ^{1}H NMR spectrum (Figure S52), suggesting that the dynamic behavior of these groups is frozen at lower temperatures.

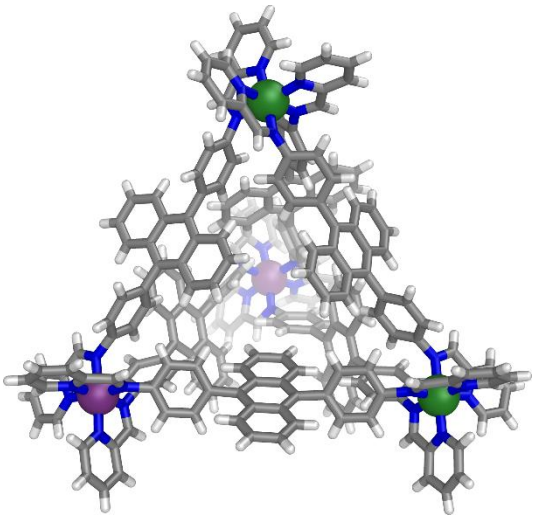

Figure 5. Cationic part of one of the two crystallographically unique cages in the crystal structure of **6**-S_4. Counterions, solvents and disorder are omitted for clarity. Δ and Λ Fe^{II} centers are colored purple and green, respectively.

X-ray quality crystals of 2,6-anthracene-edged cage **7** were obtained from vapor diffusion of diisopropyl ether into an acetonitrile solution of **7**·8NTf_2 containing excess Bu_4NPF_6. Cage **7** crystallized in the trigonal space group $R\bar{3}$ with one complete cage in the asymmetric unit. The crystals were found to contain only the achiral S_4-symmetric diastereomer (Figure 5). This diastereomer was also most abundant in solution, with an observed distribution of 8% **7**-*T*, 43% **7**-C_3 and 49% **7**-S_4. The Fe-Fe distances are in the range 20.8-21.3 Å (average 21.0 Å), significantly longer than its 1,5- and 9,10-anthracene-edged congeners **5** and **6**. The elongated anthracene panels extend along the edges of the tetrahedron, resulting in large pores of up to ca. 5 Å diameter in the surface of the cage (see Figure S154).

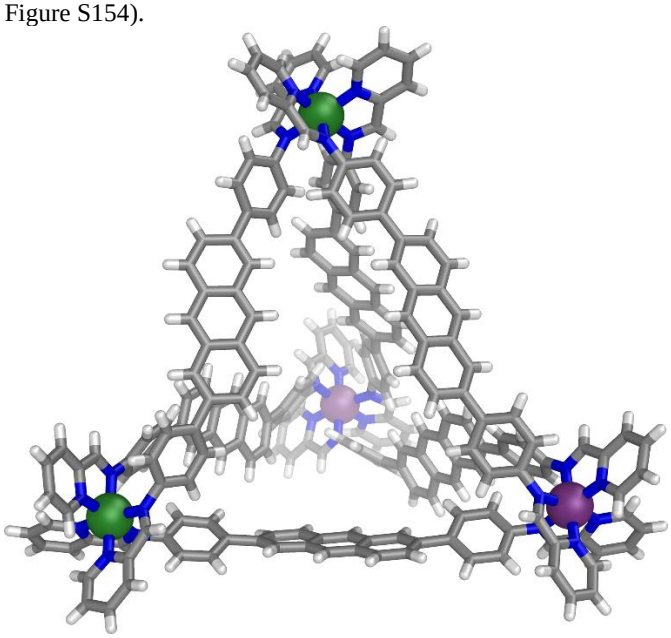

Figure 6. Cationic part of the crystal structure of **7**-S_4. Counterions, solvents and disorder are omitted for clarity. Δ and Λ Fe^{II} centers are colored purple and green, respectively.

Host-guest studies. The guest encapsulation properties of cages **1**-**7** were investigated in solution in order to probe the relationship between the sizes and shapes of the aromatic panels and the binding abilities of the cages. The scope of guest binding within the cages was investigated with a series of large hydrophobic prospective guests including fullerenes, polycyclic aromatic hydrocarbons (PAHs) and cholesterol, as a cannonical example of a structurally complex lipophilic natural product (Figure 7, Table 1). These molecules were hypothesized to interact with the aromatic spacers of the cages through a combination of aromatic stacking, CH-π interactions, van-der-Waals interactions and solvophobic effects. They have previously been shown to be encapsulated by other metal-organic cages[16] that contain large aromatic panels, including cage **8**, whose offset 1,6-pyrene scaffold was able to provide a well-enclosed cavity suitable for the encapsulation of large hydrophobic guests.[22] In contrast cage **9**, based on a linear 2,7-pyrene scaffold, had a more porous cavity and did not show affinity for these neutral hydrophobic guests.[22]

The hydrophobic cages displayed poor solubility and were unstable in aqueous solution due to their incorporation of ditopic ligands;[30] therefore we restricted our binding investigations to acetonitrile. All host-guest complexes were prepared on an NMR scale and characterized by ^{1}H, ^{13}C and DOSY NMR and ESI-MS where applicable. For each entry in Table 1 the prospective guest (2-5 equiv)[31] was added as a solid to a CD_3CN solution of the host (1-3 mM) and the mixture was allowed to equilibrate for at least 24 hours at 323 K prior to the acquisition of NMR spectra. In cases where no encapsulation was inferred to have taken place, the signals for the cage appeared at the same chemical shifts as in the absence of the guest, and the signals for the guest were identical to those in the absence of host for ^{1}H NMR active guests that were soluble in CD_3CN. Small shifts (<0.05 ppm) were attributed to weak non-specific π-stacking interactions while guest encapsulation was inferred by more significant shifts (>0.05 ppm). Fast-exchange host occupation was inferred when shifts or broadening of the host or guest NMR signals were observed. Slow-exchange host occupation was inferred to occur when a new set of cage peaks was observed at different chemical shifts, and peaks corresponding to the free host had partially or completely disappeared; a new set of signals was also observed for the encapsulated guest in the NMR spectra of the host-guest complexes. Encapsulation of these slowly exchanging guests was further confirmed by DOSY NMR, where the encapsulated guest and host were observed to diffuse at the same rate. Host-guest complexes displaying slow-exchange guest binding were further characterized by ESI-MS while those showing fast-exchange guest binding typically did not remain intact during the ESI-MS experiment.

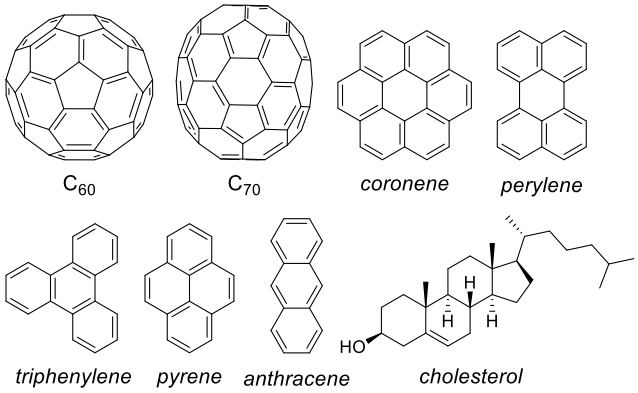

Figure 7. Prospective guests used in this study.

Table 1. Summary of the host-guest chemistry of cages 1-9 in CD_3CN.

Guest	Encapsulation observed (NMR rate of exchange at 298 K)								
	Cage **1**	Cage **2**	Cage **3**	Cage **4**	Cage **5**	Cage **6**	Cage **7**	Cage **8**[e]	Cage **9**[e]
C_{60}	Yes (slow)	No	No	No	Yes (slow)[d]	No	No	Yes (slow)	No
C_{70}	Yes (slow)	No	Yes (slow)[b]	No	Yes (slow)[d]	No	No	Yes (slow)	No
coronene	Yes (slow)	Yes (fast)	No	No	No	No	No	Yes (slow)[a]	No
perylene	Yes (fast)[a]	Yes (fast)	Yes (fast)	No	No	No	No	Yes (fast)	No
pyrene	Yes (fast)	No	No	Yes (fast)[c]	Yes (slow)[a]	Yes (fast)	No	Yes (fast)	No
triphenylene	Yes (fast)	No	No	No	Yes (fast)[a]	Yes (fast)[c]	No	Yes (fast)	No
anthracene	Yes (fast)	No	No	No	No	Yes (fast)[c]	No	Yes (fast)	No
cholesterol	Yes (fast)	Yes (fast)	No	No	Yes (fast)[a]	No	No	Yes (fast)	No

[a] Significant broadening of the host and/or guest signals was observed, suggesting an intermediate rate of exchange on the NMR timescale. Binding has been assigned as slow- or fast-exchange depending on whether a separate set of NMR signals was observed for the encapsulated guest. [b] Only partial encapsulation was observed, even after 45 days at 333 K. [c] Modest shifts of up to 0.1 ppm were observed in the guest signals, indicative of a weak, fast exchange binding process. [d] Cage **5** was reported to form a covalent Diels-alder adduct with C_{60};[24] we infer a similar adduct to be formed with C_{70}. [e] The host-guest properties of cages **8** and **9** were described previously.[22]

In most cases guest insolubility and signal overlap resulting from the stereochemical complexity of the cages[22,28] prevented quantification of binding strength through ^{1}H NMR titration; similarly UV/vis and fluorescence did not prove suitable for investigating guest binding in these systems.[32] Nevertheless clear trends in binding ability were evident within the series of cages allowing us to deduce the structural factors important for guest binding. Previous studies on rigid host-guest systems have focused on occupancy as a key determining factor for guest binding, with a total guest volume of 55 ± 9% inferred to be optimal.[34] However, in cases where the host cavity cannot be precisely defined[34] or the host is flexible,[35] the definition of cavity volume becomes less clear, as is the case here. The cage volumes depend on the stereochemical configurations (Λ/Δ) of the metal centers and the orientations of the aromatic panels. Indeed, previous DFT studies on cage **8** suggested that the host is able to adapt to accommodate guests through pyrene rotation to provide a tailored guest-binding pocket.[22] Instead of occupancy, we have focused on the size, shape, and degree of offset of the aromatic panels as the key parameters determining guest binding propensity.

Chrysene-edged cage **1** was observed to form 1:1 host-guest complexes with C_{60} and C_{70}, as indicated by ESI-MS. The addition of one of these fullerenes to **1** in CD_3CN resulted in complete conversion to [$C_{60} \subset$ **1**] or [$C_{70} \subset$ **1**] within 24 hours at 323 K, as evidenced by the disappearance of the peaks corresponding to the free host and concurrent appearance of a new set of cage peaks corresponding to the host-guest complex. Encapsulation of C_{60} by **1** was also supported by the observation of an intense resonance at 140.6 ppm in the ^{13}C NMR spectrum of [$C_{60} \subset$ **1**] in CD_3CN (Figure S72) despite the negligible solubility of C_{60} in this solvent.[36]

Examination of the imine signals in the ^{1}H NMR spectrum of [$C_{60} \subset$ **1**] showed a major species (comprising ca. 90% of the total integrated intensity) with three peaks having 1:1:2 relative integrated intensity, consistent with **1**-C_3 predominating in solution upon the binding of C_{60}. This observation contrasts with the clusters of peaks observed in the ^{1}H and ^{13}C NMR spectra of **1** in the absence of C_{60}, which showed a mixture of diastereomers in solution. Overlap between the signals within each cluster prevented quantification of the proportions of individual diastereomers for the empty cage. However, we note that **1**-S_4 was observed in the crystal and infer that this diastereomer is also likely to be present in solution. Guest binding thus brought about a re-equilibration among the different cage diastereomers. As was observed in the case of 1,6-pyrene-edged cage **8**,[22] we hypothesize that the system expresses the diastereomers that form the lowest energy host-guest complexes, for this case, **1**-C_3. We infer that this diastereomer optimally binds guests, allowing each chrysene panel to adopt a conformation tangential to the edges of the tetrahedron, thus facilitating aromatic stacking with the guest.

In contrast to the well resolved ^{1}H NMR spectrum of [$C_{60} \subset$ **1**], the ^{1}H NMR spectrum of [$C_{70} \subset$ **1**] was intractably complex, which we attribute to the lower symmetry of the C_{70} complexes (Figure S78). Any orientation adopted by the elliptical fullerene guest within the cavity of any host stereoisomer will break the NMR-reported symmetry of both host and guest unless tumbling occurs rapidly on the NMR time scale. We infer that this tumbling is slowed by the ellipticity of C_{70}, in contrast with spherical C_{60}.

In addition to binding fullerenes, cage **1** was also observed to encapsulate planar PAHs. The addition of excess coronene (5 equiv) to **1** in CD_3CN resulted in formation of a 1:2 host-guest complex as indicated by ESI-MS; no significant peaks for the free host or host-guest complexes with other stoichiometries were observed. When only one equivalent of coronene was added to **1**, empty cage **1** and the host-guest complex [(coronene)$_2 \subset$ **1**] were the major species observed by ESI-MS with only trace amounts of the 1:1 host-guest complex detected. This observation led us to infer that two equivalents of coronene bound within **1** cooperatively.

The ^{1}H NMR spectrum of [(coronene)$_2 \subset$ **1**] shows significant desymmetrization of the host signals, consistent with slow tumbling of the guests within the host on the NMR timescale. The coronene signals are shifted upfield by 3.3 ppm to 5.69 ppm upon encapsulation. The DOSY spectrum of [(coronene)$_2 \subset$ **1**] (Figure S84) confirmed that both the host and guest diffused at the same rate.

Addition of the slightly smaller perylene to **1** resulted in significant broadening of the host signals, either due to an intermediate rate of exchange between free and bound guests on the NMR timescale, or to tumbling of the bound perylenes within the host. Cooling the host-guest mixture in CD_3CN to 233 K led to a loss of the observed symmetry in the ^{1}H NMR spectrum, although dynamic behavior was not completely frozen out above the freezing point of CD_3CN.

The smaller PAHs pyrene, triphenylene and anthracene bound within **1** in fast-exchange on the NMR timescale, as inferred from small shifts in the host signals and distinct upfield shifts in the guest signals. We infer that these guests are too small to be tightly encapsulated within the cavity of **1**. Similarly, the hydrophobic steroid cholesterol was also bound by **1** in fast exchange, as indicated by shifts in the guest signals of up to 0.8 ppm upfield, relative to those of free cholesterol, and broadening of both host and guest signals.

These results indicate that the chrysene moieties of **1** provide an enclosed cavity suitable for the encapsulation of a variety of large hydrophobic guests, ranging from fullerenes and PAHs, to asymmetric natural products such as steroids. The scope of guests bound within **1** is similar to that reported for 1,6-pyrene-edged cage **8**,[22] which has similarly offset but differently shaped aromatic panels. The offset nature of the ligands may thus be an important factor in achieving the degree of enclosure required for optimization of binding.

Triphenylene-edged cage **2** is an isomer of **1**, but **2** possesses a different shape and arrangement of aromatic panels at its edges. Cage **2** was investigated as a host for the hydrophobic guests that were found to bind within **1**. No evidence was observed for the encapsulation of C_{60} or C_{70} within **2**. We infer these fullerenes to present poor size and shape matches for the cavity of **2**, and that its edges cannot readily adopt a conformation where the triphenylene panels can stack with the fullerenes.

Cage **2** was observed, however, to bind the larger PAHs coronene and perylene and the steroid cholesterol in fast exchange on the NMR timescale. This behavior contrasts with the slow/intermediate exchange binding observed for these guests with **1**. Cage **2** showed no evidence of binding the smaller PAHs pyrene, triphenylene and anthracene. We attribute the reduced guest binding ability of cage **2** relative to **1** to the cavity of **2** not being sufficiently enclosed to define a space distinct from the surrounding solvent. A similar absence of guest binding was observed for the previously-reported 2,7-pyrene-edged cage **9**,[22] which also possesses a linear ligand arrangement.

While the shapes and arrangements of the aromatic panels appear crucial to determining whether the inner cavity of a cage is sufficiently enclosed to trap guests inside, the size of the aromatic panels also appears crucial to consider. The 2,6-naphthalene moities of cage **3** are identical in length and offset geometry to the chrysene groups of **1**, differing only in the sizes of the aromatic panels and therefore in the degree of surface enclosure.

In contrast to **1**, cage **3** was not observed to encapsulate fullerene C_{60}, even after heating for 4 days at 363 K or 46 days at 333 K. However, the addition of excess C_{70} to **3** led to 21% conversion to the host-guest complex [$C_{70} \subset$ **3**] after 24 hr at 333 K, increasing to a maximum of 58% conversion after 46 days. The degree of guest encapsulation was not improved by carrying the reaction out in 1:1 MeCN/o-dichlorobenzene, a solvent mixture in which C_{70} is more soluble, although the rate of guest uptake was increased.

We infer that binding was weaker between C_{70} and **3** relative to **1** due to the smaller aromatic surface area available for aromatic stacking in the case of 2,6-naphthalene-edged **3**. The selectivity for C_{70} over C_{60} displayed by **3** may result from the greater aromatic surface area of C_{70} and its lesser curvature, allowing it to benefit from more extensive stabilizing contacts relative to C_{60}. Notably, isomeric cage **4**, based on a 1,5-naphthalene scaffold, did not encapsulate either C_{60} or C_{70}. We infer that the shorter Fe-Fe distances in **4** relative to **3** rendered the cavity too small for fullerene encapsulation.

Of the PAHs bound by cage **1**, only perylene showed evidence of a binding interaction with **3**, as indicated by shifts in the host signals, and broadening and upfield shifts in the perylene peaks. Upon cooling to 233 K, [perylene $\subset$ **3**] displayed slow exchange guest binding behavior, accompanied by splitting of the ligand phenylene protons into separate signals that corresponded to protons directed inside and outside of the cage cavity, consistent with slow rotation of the phenylene rings on the NMR timescale. This behavior contrasted with the fast phenylene rotation observed for cage **3**, even at 233 K, in the absence of guest molecules. The more limited range of guests bound by **3** relative to **1** attests to the importance of the larger chrysene panels in **1**, which act to enclose the cage inner cavity from bulk solution.

Having observed the essential role played by the offset ligands of **1** and **8** in guest binding, we sought to explore the scope and limitations of the ligand offset as a driving factor for guest binding. We recently reported 1,5-anthracene-edged cage **5** and its ability to form a unique covalently-trapped adduct with C_{60} *via* regiospecific Diels-Alder reactions of three of its six anthracene panels with a single C_{60} guest.[24] In the present study, we have explored the host-guest chemistry of **5** with the hydrophobic guests shown in Figure 7.

No evidence of encapsulation within **5** was observed for the largest PAHs, coronene and perylene. However, addition of the smaller PAHs and cholesterol resulted in significant changes to the ^{1}H NMR signals of the host and guests, consistent with host-guest interactions in solution.

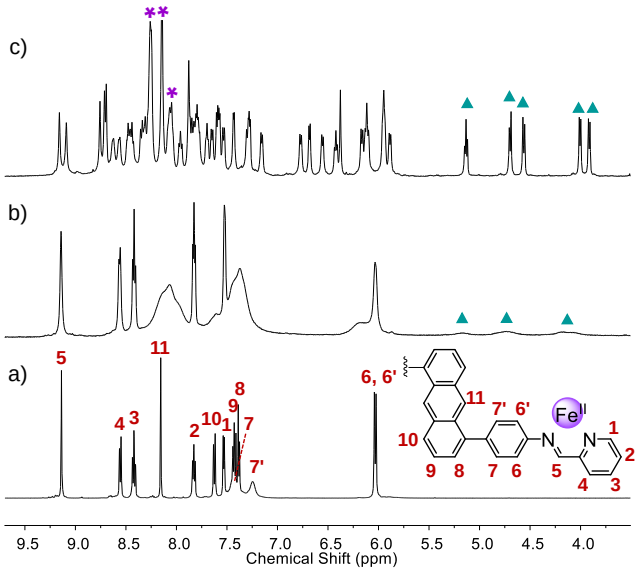

Figure 8. Partial ^{1}H NMR spectra (500 Hz, CD_3CN) of (a) *T*-symmetric cage **5** at 298 K (b) host-guest complex [$(pyrene)_2 \subset$ **5**] at 298 K (c) host-guest complex [$(pyrene)_2 \subset$ **5**] at 238 K. Cyan triangles denote bound pyrene; purple asterisks denote excess free pyrene.

The addition of excess pyrene (ca. 5 equiv) to **5** in CD_3CN resulted in broadening of the ^{1}H NMR signals of the anthracene protons of the cage, as well as the signals of excess pyrene, and the appearance of a series of broad signals in the 4.0-5.5 ppm region (Figure 8b). Cooling the host-guest mixture in CD_3CN solution to 238 K led to a sharpening and increase in the number of signals in the ^{1}H NMR spectrum (Figure 8c). This observation is consistent with desymmetrization of the host as a result of slow tumbling of the pyrene guests on the NMR timescale. The broad signals in the range 4.0-5.5 ppm region split into five sharp peaks at 238 K, assigned to the encapsulated pyrene, also desymmeterized on binding. These signals are shifted upfield by up to 4.3 ppm relative to those of free pyrene.

NMR integration suggested encapsulation of two guests per cage. The ^{1}H NMR spectrum of [$(pyrene)_2 \subset$ **5**] displayed three signals per ligand environment, in contrast to the highly symmetric ^{1}H NMR spectrum observed for empty **5**, which was observed solely as the most symmetric *T* diastereomer in solution. When only one equivalent of pyrene was added to **5**, the ^{1}H NMR spectrum of the mixture at 238 K showed only empty cage **5** and the host-guest complex [$(pyrene)_2 \subset$ **5**] suggesting that the two equivalents of pyrene bind cooperatively within the cavity of **5**.

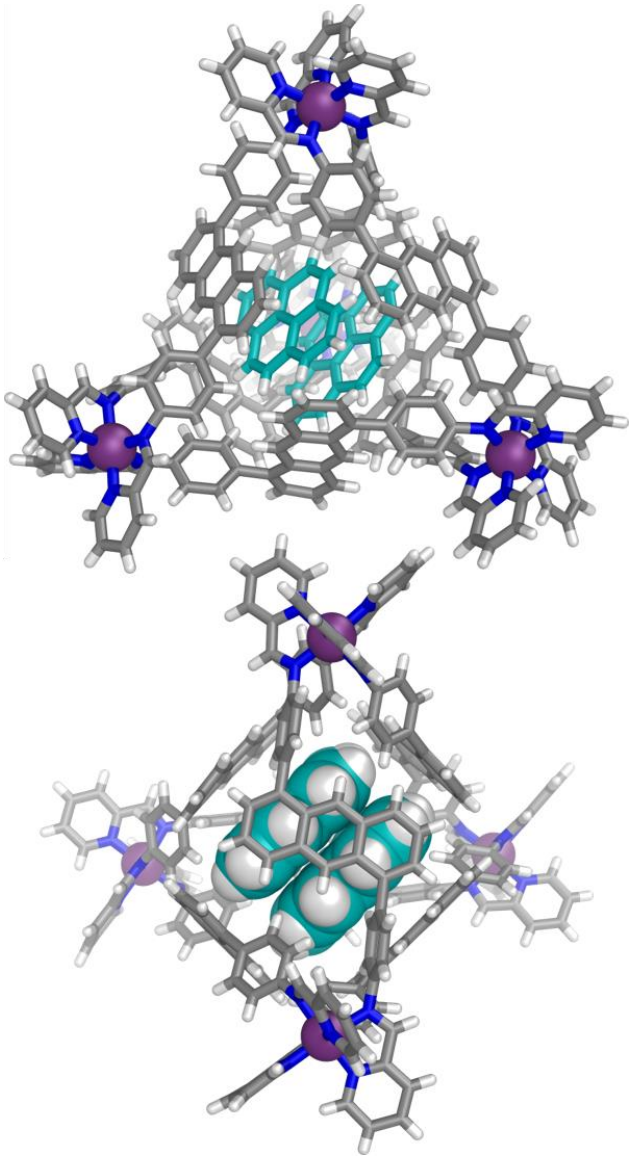

Figure 9. Views through a face (top) and an edge (bottom) of the cationic part of the crystal structure of [(pyrene)$_2$ ⊂ **5**] showing the ΛΛΛΛ enantiomer. Counterions, solvents and disorder are omitted for clarity.

The solid-state structure of [(pyrene)$_2$ ⊂ **5**] was revealed through single crystal X-ray diffraction. X-ray quality crystals were obtained from vapor diffusion of diisopropyl ether into an acetonitrile solution of [(pyrene)$_2$ ⊂ **5**]·8NTf$_2$ containing pyrene (ca. 10 equiv per cage) and excess Bu_4NClO_4. The host-guest complex crystallized in tetragonal space group I 41/a, with half of a cage molecule and one encapsulated pyrene in the asymmetric unit.

The structure consisted of a stacked dimer of pyrenes within the cavity of **5** with an interplanar distance of ca. 3.5 Å, as is typical for arene-arene interactions (Figure 9). The two molecules are rotated with respect to one another by 82°. The pyrene dimer is located centrally between two opposite cage walls, resulting in a four-component anthracene-pyrene-pyrene-anthracene stack (Figure 9) with an angle of 5.6° between the pyrene and anthracene moieties and an average distance of 3.9 Å between stacked rings. Examination of the structure of [(pyrene)$_2$ ⊂ **5**] indicates that the pyrene dimer is a good size and shape match for the cavity of **5**, occupying ca. 65% of the cavity volume. The average Fe-Fe distance in [(pyrene)$_2$ ⊂ **5**] of 17.1 Å is almost identical to the previously-reported structure of **5**, where the cavity was occupied by disordered diisopropyl ether molecules.[24]

The structure of [(pyrene)$_2$ ⊂ **5**] confirms that all iron(II) centers within each cage maintain the same Δ or Λ stereochemistry, with the observed desymmetrization at 238 K relative to **5** resulting from the well-defined stacking arrangement of the guests. The higher symmetry spectrum of [(pyrene)$_2$ ⊂ **5**] obtained at 298 K is consistent with the guests tumbling at a higher rate as the temperature is increased. In addition to this tumbling motion, we infer that pyrene is exchanging between the cavity of **5** and the bulk solution at 298 K, as indicated by broadening of the ^{1}H NMR signals for excess pyrene. Fast-exchange binding was observed at higher temperatures, as evidenced by the disappearance above 328 K of the separate signals for encapsulated pyrene (Figure S114)

The addition of triphenylene to **5** resulted in fast-exchange host occupation, as evidenced by shifts to some of the ^{1}H NMR resonances of **5** and broadening of the triphenylene signals. Upon cooling to 238 K, [triphenylene ⊂ **5**] displayed slow exchange guest binding behavior (Figure S119), accompanied by dispersion of the phenylene proton NMR signals relative to the empty cage as a result of contact with the aromatic guest.

In contrast to the host desymmetrization observed in [(pyrene)$_2$ ⊂ **5**], the triphenylene complex retains the *T* symmetry observed in the NMR of parent cage **5**. Although the pyridyl and imine protons of the host in [triphenylene ⊂ **5**] appear at almost the same chemical shifts as in empty **5**, the anthracene signals show upfield shifts of up to 0.17 ppm and the encapsulated triphenylene signal at 4.80 ppm is significantly upfield shifted relative to free triphenylene. Exchange cross-peaks between the signals for free and bound triphenylene were observed in the ^{1}H-^{1}H NOESY spectrum at 238 K. Integration of the signal for the encapsulated triphenylene relative to the cage protons indicates a 1:1 host:guest stoichiometry, in contrast to the 1:2 complex observed with pyrene.

No evidence of host-guest interaction was observed between **5** and the smaller PAH anthracene. Binding was observed, however, with cholesterol, as indicated by splitting and broadening of some host peaks and significant broadening of the cholesterol peaks, consistent with tumbling of the guest within the host on the NMR timescale. These peaks sharpened slightly upon heating to 318 K, consistent with an increased tumbling rate at higher temperatures (Figure S128). Cooling a mixture of cholesterol and **5** to 233 K led to further desymmetrization of the host signals and some sharpening of the guests signals, with downfield shifts of up to 3.55 ppm relative to the free guest.

Despite the difference between the ligands of **5** and **4** of only one fused benzene ring, **4** showed no NMR evidence of binding triphenylene or cholesterol, and only weak evidence of binding pyrene in fast exchange, as indicated by shifts of up to 0.1 ppm in the guest signals and minimal changes in the host signals. The more enclosed surface of **5** (pores of ca. 1.4 Å) relative to **4** (pores of ca. 2.0 Å) thus plays an essential role in enabling guest encapsulation.

Similarly, the 9,10-anthracene edged cage **6** was a less effective host than **5**. Cage **6** did not show any interaction with cholesterol and displayed only fast exchange binding behavior with pyrene, triphenylene and anthracene at 298 K. In contrast

to **5**, cage **6** was not observed to undergo Diels-Alder reaction with C_{60}. We infer that **6** may not be able to adopt a conformation where the anthracene panels can align with the fullerene with the registry required for Diels-Alder reaction.

The third isomeric cage **7**, based on 2,6-anthracenyl panels, was not observed to interact with any of the prospective guests shown in Figure 7. We attribute the absence of guest binding within **7**, compared to its isomers **5** and **6**, to the cavity of **7** not being sufficiently enclosed to isolate the cavity from the solvent environment. The 2,6-anthracenyl connectivity within **7** appears to engender a poor size and shape match for C_{60} and C_{70}, preventing all six ligands from simultaneously interacting with the fullerene. The anthracenyl cage with the largest degree of offset, cage **5**, thus has the optimum degree of cavity enclosure for effective guest binding.

Conclusions

This study elucidates the parameters governing guest binding within a class of aromatic-paneled $Fe^{II}_4L_6$ cages prepared from building blocks with different geometries. The host-guest properties of the cages were strongly dependent on the size and arrangement of the aromatic panels composing the cage surface. Ligand offset was found to determine the degree of surface enclosure, which in turn dictates guest binding propensity.

Chrysene-edged cage **1** was found to display the widest scope of guest binding. It bound fullerenes and large PAHs in slow exchange, and smaller hydrophobic guests in fast exchange. An isomeric triphenylene-edged cage **2** had a similar ligand surface area but a more open cavity than **1**, and a 2,6-naphthalene edged cage **3** had nearly identical M-M distances to **1** but smaller aromatic panels. Both **2** and **3** were much less effective hosts than **1**, demonstrating the importance of cavity enclosure for strong host-guest interactions. Comparison between the three isomeric anthracene-edged cages **5**-**7** also revealed very different host-guest properties depending on the arrangement of the anthracene groups around the surface of the tetrahedra. Cage **5**, with 1,5-anthracene edges, provided the most enclosed cavity for effective guest binding. Cages **4** and **5** had similar cavity sizes, but the smaller aromatic panels and the larger surface pores of 1,5-naphthalene edged cage **4** rendered it a less effective host than **5**.

These results show that when designing metal-organic hosts, the following considerations can bring about more effective guest encapsulation: (i) offset ligands are most efficient at enclosing surfaces; (ii) larger aromatic panels are better than smaller ones and (iii) small changes in the length, shape and geometry of the aromatic panels have large effects upon guest-binding ability. This set of design principles may help guide the construction of new hosts to be integrated into host-guest systems with tailored functions.

ASSOCIATED CONTENT

The Supporting Information is available free of charge on the ACS Publications website at DOI:
X-ray data for **1** (CCDC 1541836) (CIF).
X-ray data for **2** (CCDC 1541837) (CIF).
X-ray data for **3** (CCDC 1541838) (CIF).
X-ray data for **4** (CCDC 1541839) (CIF).
X-ray data for **6** (CCDC 1541840) (CIF).
X-ray data for **7** (CCDC 1541841) (CIF).
X-ray data for [(pyrene)$_2$ ⊂ **5**] (CCDC 1541842) (CIF).
Synthetic details, characterization data, NMR and mass spectra (PDF).

AUTHOR INFORMATION

Corresponding Author

* jrn34@cam.ac.uk.

Author Contributions

All authors have given approval to the final version of the manuscript.

Notes

The authors declare no competing financial interests.

ACKNOWLEDGMENT

This work was supported by the UK Engineering and Physical Sciences Research Council (EPSRC, EP/M01083X/1). We thank the EPSRC Mass Spectrometry Service at Swansea for carrying out high resolution mass spectrometry and Diamond Light Source (UK) for synchrotron beamtime on I19 (MT11397). We also thank the NMR service team at the Department of Chemistry, University of Cambridge for performing some NMR experiments

REFERENCES

(1) (a) Cook, T. R.; Stang, P. J. *Chem. Rev.* **2015**, *115*, 7001. (b) Chakrabarty, R.; Mukherjee, P. S.; Stang, P. J. *Chem. Rev.* **2011**, *111*, 6810. (c) Fujita, D.; Ueda, Y.; Sato, S.; Mizuno, N.; Kumasaka, T.; Fujita, M. *Nature* **2016**, *540*, 563. (d) Henkelis, J. J.; Hardie, M. J. *Chem. Commun.* **2015**, *51*, 11929. (e) Xu, L.; Wang, Y.-X.; Yang, H.-B. *Dalton Trans.* **2015**, *44*, 867. (f) Pasquale, S.; Sattin, S.; Escudero-Adán, E. C.; Martínez-Belmonte, M.; de Mendoza, J. *Nat. Commun.* **2012**, *3*, 785. (g) Han, M.; Engelhard, D. M.; Clever, G. H. *Chem. Soc. Rev.* **2014**, *43*, 1848. (h) Ward, M. D. *Chem. Commun.* **2009**, 4487. (i) Harris, K.; Fujita, D.; Fujita, M. *Chem. Commun.* **2013**, *49*, 6703.

(2) (a) Jordan, J. H.; Gibb, B. C. *Chem. Soc. Rev.* **2015**, *44*, 547. (b) Evans, J. D.; Sumby, C. J.; Doonan, C. J. *Chem. Lett.* **2015**, *44*, 582. (c) Zhang, G.; Mastalerz, M. *Chem. Soc. Rev.* **2014**, *43*, 1934. (d) Yoshizawa, M.; Klosterman, J. K. *Chem. Soc. Rev.* **2014**, *43*, 1885. (e) Diaz-Moscoso, A.; Ballester, P. *Chem. Commun.* **2017**, *53*, 4635. (f) Leenders, S. H. A. M.; Gramage-Doria, R.; de Bruin, B.; Reek, J. N. H. *Chem. Soc. Rev.* **2015**, *44*, 433.

(3) (a) Zhang, W.-Y.; Lin, Y.-J.; Han, Y.-F.; Jin, G.-X. *J. Am. Chem. Soc.* **2016**, *138*, 10700. (b) Bloch, W. M.; Abe, Y.; Holstein, J. J.; Wandtke, C. M.; Dittrich, B.; Clever, G. H. *J. Am. Chem. Soc.* **2016**, *138*, 13750. (c) Preston, D.; Lewis, J. E. M.; Crowley, J. D. *J. Am. Chem. Soc.* **2017**, *139*, 2379. (d) Custelcean, R.; Bonnesen, P. V.; Duncan, N. C.; Zhang, X.; Watson, L. A.; Van Berkel, G.; Parson, W. B.; Hay, B. P. *J. Am. Chem. Soc.* **2012**, *134*, 8525.

(4) Galan, A.; Ballester, P. *Chem. Soc. Rev.* **2016**, *45*, 1720.

(5) Riddell, I. A.; Smulders, M. M. J.; Clegg, J. K.; Nitschke, J. R. *Chem. Commun.* **2011**, *47*, 457.

(6) (a) García-Simón, C.; Garcia-Borràs, M.; Gómez, L.; Parella, T.; Osuna, S.; Juanhuix, J.; Imaz, I.; Maspoch, D.; Costas, M.; Ribas, X. *Nat. Commun.* **2014**, *5*, 5557. (b) Kishi, N.; Akita, M.; Yoshizawa, M. *Angew. Chem. Int. Ed.* **2014**, *53*, 3604. (c) Frischmann, P. D.; Mehr, S. H. M.; Patrick, B. O.; Lelj, F.; MacLachlan, M. J. *Inorg. Chem.* **2012**, *51*, 3443.

(7) Wu, K.; Li, K.; Hou, Y.-J.; Pan, M.; Zhang, L.-Y.; Chen, L.; Su, C.-Y. *Nat. Commun.* **2016**, *7*, 10487.

(8) (a) Cullen, W.; Misuraca, M. C.; Hunter, C. A.; Williams, N. H.; Ward, M. D. *Nat. Chem.* **2016**, *8*, 231. (b) Levin, M. D.; Kaphan, D. M.; Hong, C. M.; Bergman, R. G.; Raymond, K. N.; Toste, F. D. *J. Am. Chem. Soc.* **2016**, *138*, 9682. (c) Howlader, P.; Das, P.; Zangrando, E.; Mukherjee, P. S. *J. Am. Chem. Soc.* **2016**, *138*, 1668.

(d) Marcos, V.; Stephens, A. J.; Jaramillo-Garcia, J.; Nussbaumer, A. L.; Woltering, S. L.; Valero, A.; Lemonnier, J.-F.; Vitorica-Yrezabal, I. J.; Leigh, D. A. *Science* **2016**, *352*, 1555.

(9) (a) Frischmann, P. D.; Kunz, V.; Würthner, F. *Angew. Chem. Int. Ed.* **2015**, *54*, 7285. (b) Shanmugaraju, S.; Mukherjee, P. S. *Chem. Eur. J.* **2015**, *21*, 6656.

(10) (a) Yoshizawa, M.; Takeyama, Y.; Kusukawa, T.; Fujita, M. *Angew. Chem. Int. Ed.* **2002**, *41*, 1347. (b) Yoshizawa, M.; Miyagi, S.; Kawano, M.; Ishiguro, K.; Fujita, M. *J. Am. Chem. Soc.* **2004**, *126*, 9172.

(11) Zheng, Y.-R.; Zhao, Z.; Kim, H.; Wang, M.; Ghosh, K.; Pollock, J. B.; Chi, K.-W.; Stang, P. J. *Inorg. Chem.* **2010**, *49*, 10238.

(12) (a) Li, K.; Zhang, L.-Y.; Yan, C.; Wei, S.-C.; Pan, M.; Zhang, L.; Su, C.-Y. *J. Am. Chem. Soc.* **2014**, *136*, 4456. (b) Spenst, P.; Sieblist, A.; Würthner, F. *Chem. Eur. J.* **2017**, *23*, 1667. (c) Yang, L.; Jing, X.; He, C.; Chang, Z.; Duan, C. *Chem. Eur. J.* **2016**, *22*, 18107. (d) Szaloki, G.; Croue, V.; Allain, M.; Goeb, S.; Salle, M. *Chem. Commun.* **2016**, *52*, 10012. (e) Singh, N.; Jo, J.-H.; Song, Y. H.; Kim, H.; Kim, D.; Lah, M. S.; Chi, K.-W. *Chem. Commun.* **2015**, *51*, 4492. (f) Juríček, M.; Barnes, J. C.; Dale, E. J.; Liu, W.-G.; Strutt, N. L.; Bruns, C. J.; Vermeulen, N. A.; Ghooray, K. C.; Sarjeant, A. A.; Stern, C. L.; Botros, Y. Y.; Goddard, W. A.; Stoddart, J. F. *J. Am. Chem. Soc.* **2013**, *135*, 12736. (g) Dale, E. J.; Vermeulen, N. A.; Thomas, A. A.; Barnes, J. C.; Juríček, M.; Blackburn, A. K.; Strutt, N. L.; Sarjeant, A. A.; Stern, C. L.; Denmark, S. E.; Stoddart, J. F. *J. Am. Chem. Soc.* **2014**, *136*, 10669. (h) Martínez-Agramunt, V.; Ruiz-Botella, S.; Peris, E. *Chem. Eur. J.* **2017**, *23*, 6675.

(13) Kim, K.-H.; Jahan, S. A.; Kabir, E.; Brown, R. J. C. *Environ. Int.* **2013**, *60*, 71.

(14) (a) Klein, C.; Gütz, C.; Bogner, M.; Topić, F.; Rissanen, K.; Lützen, A. *Angew. Chem. Int. Ed.* **2014**, *53*, 3739. (b) Chen, S.; Li, K.; Zhao, F.; Zhang, L.; Pan, M.; Fan, Y.-Z.; Guo, J.; Shi, J.; Su, C.-Y. *Nat. Commun.* **2016**, *7*, 13169. (c) Chan, A. K.-W.; Lam, W. H.; Tanaka, Y.; Wong, K. M.-C.; Yam, V. W.-W. *Proc. Natl. Acad. Sci. U. S. A.* **2015**, *112*, 690.

(15) Ramsay, W. J.; Szczypiński, F. T.; Weissman, H.; Ronson, T. K.; Smulders, M. M. J.; Rybtchinski, B.; Nitschke, J. R. *Angew. Chem. Int. Ed.* **2015**, *54*, 5636.

(16) (a) Mahata, K.; Frischmann, P. D.; Würthner, F. *J. Am. Chem. Soc.* **2013**, *135*, 15656. (b) Mirtschin, S.; Slabon-Turski, A.; Scopelliti, R.; Velders, A. H.; Severin, K. *J. Am. Chem. Soc.* **2010**, *132*, 14004. (c) Nakamura, T.; Ube, H.; Miyake, R.; Shionoya, M. *J. Am. Chem. Soc.* **2013**, *135*, 18790.

(17) Kishi, N.; Li, Z.; Yoza, K.; Akita, M.; Yoshizawa, M. *J. Am. Chem. Soc.* **2011**, *133*, 11438.

(18) (a) Young, M. C.; Holloway, L. R.; Johnson, A. M.; Hooley, R. J. *Angew Chem Int Ed* **2014**, *53*, 9832. (b) Ren, D.-H.; Qiu, D.; Pang, C.-Y.; Li, Z.; Gu, Z.-G. *Chem. Commun.* **2015**, *51*, 788. (c) Roberts, D. A.; Pilgrim, B. S.; Cooper, J. D.; Ronson, T. K.; Zarra, S.; Nitschke, J. R. *J. Am. Chem. Soc.* **2015**, *137*, 10068. (d) Black, S. P.; Wood, D. M.; Schwarz, F. B.; Ronson, T. K.; Holstein, J. J.; Stefankiewicz, A. R.; Schalley, C. A.; Sanders, J. K. M.; Nitschke, J. R. *Chem. Sci.* **2016**, *7*, 2614.

(19) (a) Yi, S.; Brega, V.; Captain, B.; Kaifer, A. E. *Chem. Commun.* **2012**, *48*, 10295. (b) Luo, D.; Zhou, X.-P.; Li, D. *Inorg. Chem.* **2015**, *54*, 10822. (c) Lewing, D.; Koppetz, H.; Hahn, F. E. *Inorg. Chem.* **2015**, *54*, 7653. (d) Saha, M. L.; Zhou, Z.; Stang, P. J. *Chem. Asian J.* **2016**, *11*, 2662. (e) Sham, K.-C.; Yiu, S.-M.; Kwong, H.-L. *Inorg. Chem.* **2013**, *52*, 5648.

(20) Campbell, V. E.; Nitschke, J. R. *Synlett* **2008**, 3077.

(21) Ronson, T. K.; Zarra, S.; Black, S. P.; Nitschke, J. R. *Chem. Commun.* **2013**, *49*, 2476.

(22) Ronson, T. K.; League, A. B.; Gagliardi, L.; Cramer, C. J.; Nitschke, J. R. *J. Am. Chem. Soc.* **2014**, *136*, 15615.

(23) Miyaura, N.; Suzuki, A. *Chem. Rev.* **1995**, *95*, 2457.

(24) Ronson, T. K.; Pilgrim, B. S.; Nitschke, J. R. *J. Am. Chem. Soc.* **2016**, *138*, 10417.

(25) (a) Stang, P. J.; Olenyuk, B.; Muddiman, D. C.; Smith, R. D. *Organometallics* **1997**, *16*, 3094. (b) Saalfrank, R. W.; Demleitner, B.; Glaser, H.; Maid, H.; Bathelt, D.; Hampel, F.; Bauer, W.; Teichert, M. *Chem. Eur. J.* **2002**, *8*, 2679.

(26) Saalfrank, R. W.; Maid, H.; Scheurer, A.; Puchta, R.; Bauer, W. *Eur. J. Inorg. Chem.* **2010**, *2010*, 2903.

(27) Beissel, T.; Powers, R. E.; Parac, T. N.; Raymond, K. N. *J. Am. Chem. Soc.* **1999**, *121*, 4200.

(28) (a) Meng, W.; Clegg, J. K.; Thoburn, J. D.; Nitschke, J. R. *J. Am. Chem. Soc.* **2011**, *133*, 13652. (b) Clegg, J. K.; Cremers, J.; Hogben, A. J.; Breiner, B.; Smulders, M. M. J.; Thoburn, J. D.; Nitschke, J. R. *Chem. Sci.* **2013**, *4*, 68.

(29) Ousaka, N.; Grunder, S.; Castilla, A. M.; Whalley, A. C.; Stoddart, J. F.; Nitschke, J. R. *J. Am. Chem. Soc.* **2012**, *134*, 15528.

(30) Percástegui, E.; Mosquera, J.; Nitschke, J. R. *Angew. Chem. Int. Ed.*, 10.1002/anie.201705093.

(31) In most cases guest solubility was the limiting factor in determining the quantity of guest present in solution.

(32) As noted previously for cages **8** and **9**, UV-Vis spectra were observed to undergo only minimal changes upon guest binding, and the fluorescence of the aromatic panels was quenched by the Fe^{II} centers in the cages. Hence, these techniques were also not suitable for quantifying guest binding in cages **1**-**7**.

(33) (a) Ams, M. R.; Ajami, D.; Craig, S. L.; Yang, J.-S.; Rebek Jr., J. *J. Am. Chem. Soc.* **2009**, *131*, 13190. (b) Turega, S.; Cullen, W.; Whitehead, M.; Hunter, C. A.; Ward, M. D. *J. Am. Chem. Soc.* **2014**, *136*, 8475.

(34) Mecozzi, S.; Rebek, J., Jr. *Chem. Eur. J.* **1998**, *4*, 1016.

(35) Bolliger, J. L.; Ronson, T. K.; Ogawa, M.; Nitschke, J. R. *J. Am. Chem. Soc.* **2014**, *136*, 14545.

(36) Semenov, K. N.; Charykov, N. A.; Keskinov, V. A.; Piartman, A. K.; Blokhin, A. A.; Kopyrin, A. A. *J. Chem. Eng. Data* **2009**, *55*, 13.

Table of Contents artwork